

SIMULATING VORTEX WAKES OF FLAPPING PLATES

J.X. SHENG^{*}, A. YSASI[†], D. KOLOMENSKIY[‡], E. KANSO[†],
M. NITSCHKE(✉)[§], AND K. SCHNEIDER[¶]

Abstract. We compare different models to simulate two-dimensional vortex wakes behind oscillating plates. In particular, we compare solutions using a vortex sheet model and the simpler Brown–Michael model to solutions of the full Navier–Stokes equations obtained using a penalization method. The goal is to determine whether simpler models can be used to obtain good approximations to the form of the wake and the induced forces on the body.

Key words. Separated shear flows, vortex sheets, Brown–Michael, penalization method

AMS(MOS) subject classifications. Primary 76B47

1. Introduction. A key component to better understand the locomotion and efficiency of swimming fish is the study of vortex separation, its subsequent evolution and its interaction with the moving body. Several studies have focused on the problem of flow past flapping plates. Of interest is, for example, the shape of the vortex wake as a function of the plate’s oscillation profile, as well as the resulting forces on the plate.

Recent experimental work includes soap film experiments by Schnipper et al. [22], who found a variety of wake types as a function of the generating parameters, and particle image velocimetry measurements by Godoy-Diana et al. [9]. They observed the transition between drag and thrust producing motions. The associated wake signatures, often referred to as von Karman vs. reversed von Karman wakes, have been widely studied (see e.g. [25]). Numerical simulations have followed several approaches. Examples of full Navier–Stokes simulations of flow past flapping bodies, using either compact finite difference, mixed Fourier/finite difference, or viscous vortex particle methods, are given in [2, 7, 12, 27]. Inviscid vortex sheet separation models [1, 15, 16, 18, 23, 24] are less costly since the problem is reduced to a lower-dimensional one. They are meant to be a good approximation of the outer flow away from viscous boundary layers and have been used extensively to study, for example, flapping flags in a crossflow, the motion of falling cards,

^{*}M2P2 CNRS, Aix-Marseille Université, 13453 Marseille, France

ETH Zurich, 8092 Zurich, Switzerland shengj@ethz.ch

[†]University of Southern California, Los Angeles, CA 90089, USA

[‡]M2P2 CNRS, Aix-Marseille Université, 13453 Marseille, France

Centre Européen de Recherche et de Formation Avancée en Calcul Scientifique (CERFACS), Toulouse, France

[§]Corresponding author. Department of Mathematics and Statistics, University of New Mexico, Albuquerque, NM 87131, USA

[¶]M2P2 CNRS, Aix-Marseille Université, 13453 Marseille, France

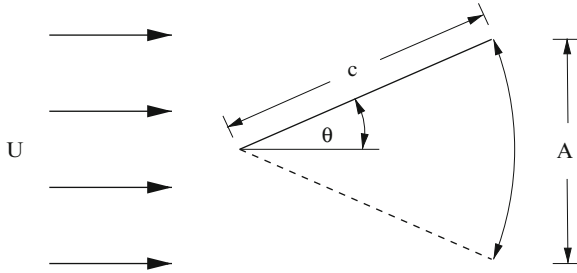


FIG. 1. Sketch illustrating the plate of length c hinged at one point, and flapping with maximal amplitude A in a background flow of magnitude U

and wakes of plates and flexible membranes. The most computationally efficient wake models are point vortex models [4, 6, 8, 17, 28].

In this paper we compare full Navier-Stokes simulations to the computationally simpler vortex sheet and point vortex approximations. The goal is to determine to what extent the wakes and resulting body forces are recovered by the simpler models. Similar comparisons of viscous and inviscid point vortex or vortex sheet approximations are also presented in [8, 19]. Such studies are needed to determine whether the simpler models can be used to improve understanding of how fish swim and steer themselves by manipulating the surrounding fluid [10, 11].

2. Problem Description. Figure 1 illustrates the problem considered here. An idealized rigid plate of zero thickness immersed in a fluid of kinematic viscosity ν is hinged at one point in an oncoming parallel flow with speed U . The plate has length c and oscillates with angle θ about a line parallel to the oncoming flow, with maximal tip displacement A . The plate motion is described by $\theta(t) = \theta_m \sin(2\pi t/\tau)$, where $\theta_m = \sin^{-1}(A/(2c))$. The governing dimensionless parameters are

$$Re = \frac{cU}{\nu}, \quad St = \frac{fA}{U}, \quad A_c = \frac{A}{c}. \quad (1)$$

Throughout this paper we consider, as an illustration, the values $St = 0.4$ with $A_c = 0.8$. Biologists have found that larger swimming fish, namely cetaceans such as dolphins and wales, swim in the range $0.25 \leq St \leq 0.35$, even though associated Reynolds numbers vary by a factor of 10 [20, 26]. The value chosen here is slightly above the observed range. We note that, for fixed f and A , the larger the Strouhal number is, the slower is the background velocity U . This causes the vorticity shed from the plate to remain near and interact longer with the plate, which increases the computational difficulty in resolving the flow. The results below are thus in the more computationally difficult regime of the observed values.

3. Numerical Methods. We simulate the fluid flow using three numerical models of increasing simplicity. In the first model, the plate is

replaced by one of finite thickness, and the flow approximated by the penalized Navier–Stokes equations [3, 21],

$$\partial_t \mathbf{u} + \mathbf{u} \cdot \nabla \mathbf{u} + \nabla p - \nu \Delta \mathbf{u} + \frac{1}{\eta} \chi_\Omega (\mathbf{u} - \mathbf{u}_p) = 0, \quad (2)$$

where $\nabla \cdot \mathbf{u} = 0$ and the density has been normalized to 1. Here, χ_Ω is a mask function which is 1 inside the region Ω occupied by the plate, and 0 elsewhere, and \mathbf{u}_p is the plate velocity. As $\eta \rightarrow 0$, the solution of (2) converges to the solution of the Navier–Stokes equations in the complement of Ω [5]. Following [14], (2) is solved on a periodic domain using a classical Fourier pseudo-spectral method for the spatial discretization, and an adaptive second order Adams–Bashforth method for the time discretization. The results presented below were obtained for fixed $Re = 1,000$, plate thickness $1/(16c)$, and $\eta = 0.001$, using $N_x \times N_y = 8,192 \times 4,096$ grid points on the computational domain $[0, 24] \times [-8, 4]$, where the plate is placed at $y = 0$.

In the vortex sheet model the fluid is treated as a purely inviscid one. The plate is modeled as a bound vortex sheet that satisfies zero normal flow through the plate. A point vortex is released at each time step from the trailing edge, and the shed vorticity is modeled as a regularized free sheet [13]. No separation is allowed at the leading edge. A key component is the algorithm used to determine the shed circulation $\Gamma(t)$. Here, we follow [18] and impose the Kutta condition

$$\frac{d\Gamma}{dt} = -\frac{1}{2}(u_+^2 - u_-^2), \quad (3)$$

where u_\pm are the tangential velocities above and below the plate, at the trailing edge. An alternative method introduced by Jones [15] is based on representing the flow in the complex plane (see also [1, 16, 23, 24]). We confirmed that the two methods give identical results for an example presented in [15], even though the implementation details differ significantly. The vortex sheet model depends on the regularization parameter for the free sheet, which in the results below is set to $\delta = 0.04c$.

The simplest model we consider is the Brown–Michael point vortex model [6, 8, 17, 28]. Here, a single point vortex is shed from the edge of the plate at the beginning of the motion. Its circulation and position changes in time so as to satisfy the Kutta condition, that is, flow tangency at the edge. At the instant the rate of change of the vortex circulation vanishes it is released: it moves with the fluid velocity and its circulation remains constant. At the same time another vortex is shed from the edge and the process repeats. The advantage of this method is that it is extremely fast.

4. Numerical Results. Figures 2–4 present the numerical results computed with the three methods, using $St = 0.4$, $A_c = 0.8$, normalized by c , at $t/\tau = 1, 2, 5$. Figure 2 plots vorticity contours computed with the

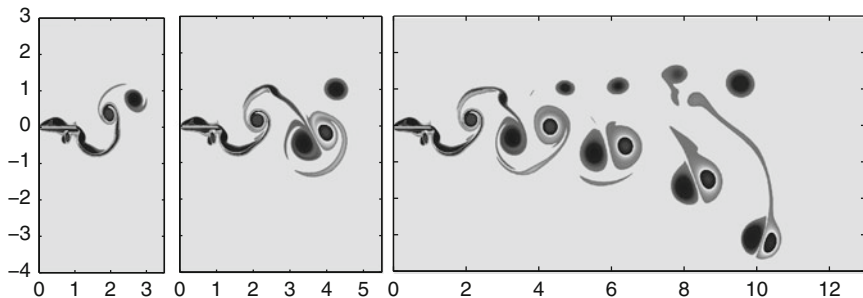


FIG. 2. *Vorticity contours of the solution to the penalized Navier-Stokes equations, for $Re = 1,000$, at $t/\tau = 1, 2, 5$*

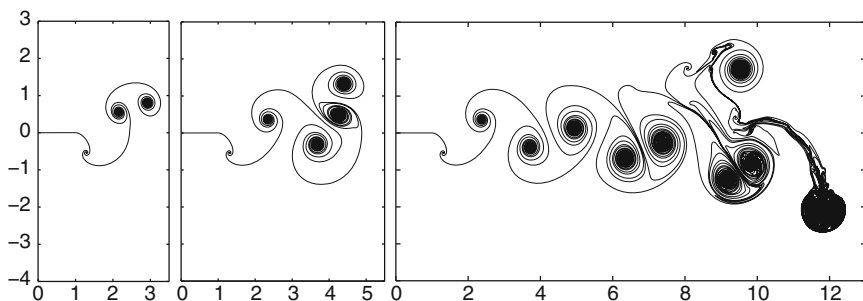


FIG. 3. *Vortex sheet position at $t/\tau = 1, 2, 5$*

Navier–Stokes penalization method, for $Re = 1,000$. Darkly colored vortex regions denote vortices of negative vorticity, regions colored in light grey with a white ring and dark interior denote vortices of positive vorticity. The vorticity values range from -50 to 50 .

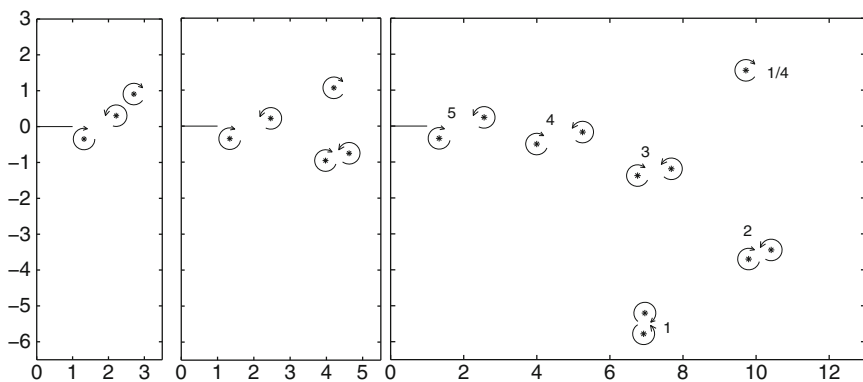


FIG. 4. *Point vortex positions computed using Brown-Michael model, at $t/\tau = 1, 2, 5$*

The plate is impulsively started from the horizontal position $\theta = 0$ with positive velocity. In the first $1/4$ period upward sweep, negative vorticity separates from the upper side of the plate, forming a vortex of negative circulation. This is the leading vortex in the first frame in Fig. 2, centered around $x = 3$. As can be seen from the second and third frame, this lead vortex travels downstream in time but remains centered above $y = 0$, by itself. With each consecutive down- and upward sweeps of the plate, two vortices of opposite sign are shed. Unlike the first, these two vortices pair up and travel diagonally downwards. For example, at $t/\tau = 2$, one well-developed pair is observed, with a second nascent one near the edge of the plate. At $t/\tau = 5$, four vortex pairs are observed, with a fifth nascent one near the edge. The leading pair at $t/\tau = 5$ is beginning to move backwards.

Note also that vorticity is generated along the walls of the plate which, at the times shown, separates from the bottom wall. Furthermore, the shear layer connecting consecutive vortex pairs begins to roll up, forming smaller secondary vortices lined up above the vortex pairs. We have performed further computations which indicate that the strength of these secondary vortices depends on the plate thickness. This is consistent with experimental results by Schnipper et al. [22]. Their Fig. 3d, e, f, all with the same value of the Strouhal number as defined in (1), indicate that by increasing the width of the leading edge in their case, the number and strength of secondary vortices per flapping cycle increases.

Figure 3 plots the position of the sheet computed with the inviscid vortex sheet model. The wall vorticity is absent, as well as the secondary vortices, but the location of the primary vortices is in good agreement with the viscous simulations. Some differences are noticeable at later times. For example, at $t/\tau = 5$ the vortex pairs travel at an angle that is less inclined, and do not travel as far downward as in the viscous case. This may be attributed to the fact that, as the viscous vortices evolve, their strength decays by diffusion changing the relative circulation between them. As a result, the leading viscous vortices are relatively weaker and may be convected more strongly by vortices behind them.

Figure 4 plots the position of the point vortices computed with the Brown–Michael model. This simple model captures the pairing of shed vortices and approximate travel direction very well. The position of the first vortex, denoted by “1/4”, is in good agreement with the other methods. Differences can be observed at $t/\tau = 5$. For example, the first vortex pair, denoted by “1”, has travelled down and backwards further than in Figs. 2 or 3. Also the second and third pairs, denoted by “2” and “3”, have travelled down further than in Fig. 2. This contrasts the vortex sheet results, in which these vortices have travelled down less than in Fig. 2.

Figures 5a, b compare the normalized shed circulation $\Gamma(t)/(Uc)$ and drag force $F_x/(U^2c)$ for the three methods. In the vortex sheet case, the force is computed following [1, 15, 24]; for the Brown–Michael model, the formulation for the force is derived following the outline given in [17].

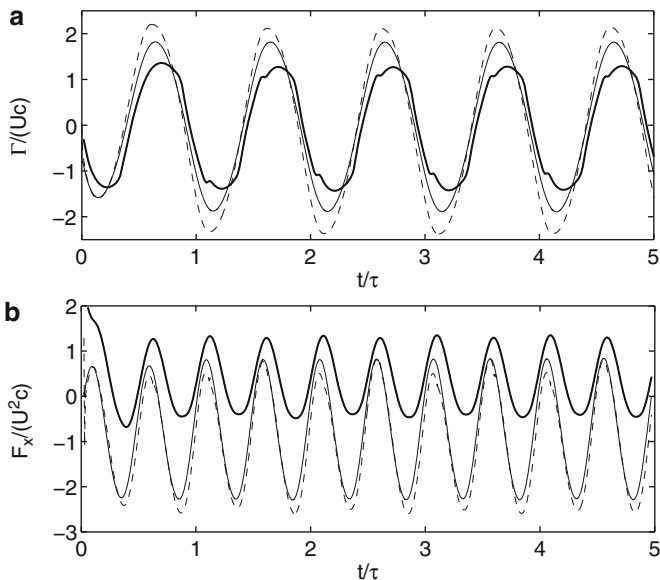


FIG. 5. (a) Normalized shed circulation $\Gamma(t)/(Uc)$, and (b) normalized drag force $C_d = F_x/(U^2c)$. Each plot shows results of the viscous simulation (thick), the vortex sheet simulation (thin) and the Brown-Michael model (dashed)

Both circulation and drag synchronize closely with the oscillation of the plate. In all models, the circulation oscillates about approximately zero mean value. The oscillation amplitudes are about 1.4–1.7 times larger in both inviscid models than in the viscous one. It is interesting that even though the circulation in the two inviscid models is quite similar, the corresponding vortex positions differ in comparison with the viscous ones. Whether this depends on the distribution of vorticity between vortices or the initial vortex placement remains to be understood. It is also curious that the viscous values in Fig. 5 lag a small time behind the other two.

In the case of the drag force in Fig. 5b, the oscillation amplitude is about 1.8 times larger in the inviscid models than in the viscous one. More significantly, however, is that the mean values of the oscillation disagree. In the inviscid models it is negative, predicting a net thrust of -0.72 (vortex sheet) to -0.95 (Brown–Michael). In the viscous model the mean drag is positive, predicting a net drag of about 0.45. Further investigation of the pressure component and the viscous component of the force, and of simpler cases for which theoretical results are available, may help elucidate which one is responsible for this discrepancy.

5. Summary. We compared simulations of the vortex wake behind a flapping plate using three models: the viscous penalized Navier–Stokes equations, a vortex sheet model, and a point vortex model. We find that

the wake structure is qualitatively similar in all three models, and the shed circulation and drag coefficient are of the same order of magnitude. There are differences in the vortex position that become more apparent at larger times. Also, in the inviscid models, the shed circulation values are larger, as is the drag oscillation amplitude. Most interestingly, the skin drag seems to dominate the horizontal force in the viscous case and not in the inviscid one. However, we have presented results for only one value of Re , plate thickness, and δ , and further study is necessary to determine the effect of these parameters on the observed differences.

Acknowledgement. The work of AY and EK is supported by the NSF CAREER award CMMI 06-44925 and the grant CCF08-11480.

REFERENCES

- [1] Alben S (2010) Passive and active bodies in vortex-street wakes. *J Fluid Mech* 642:92–125
- [2] Alben S, Shelley M (2005) Coherent locomotion as an attracting state for a free flapping body. *PNAS* 102:11163–11166
- [3] Angot P, Bruneau C-H, Fabrie P (1999) A penalization method to take into account obstacles in incompressible viscous flows. *Numer Math* 81:497–520
- [4] Aref H, Stremler M, Ponta F (2006) Exotic vortex wakes – point vortex solutions. *J Fluids Struct* 22:929–940
- [5] Carbou G, Fabrie P (2003) Boundary layer for a penalization method for viscous incompressible flow. *Adv Differ Equ* 8:1453–1480
- [6] Cortezzi L, Leonard A (1993) Point vortex model of the unsteady separated flow past a semi-infinted plate with transverse motion. *Fluid Dyn Res* 11:264–295
- [7] Eldredge JD (2005) Efficient tools for the simulation of flapping wing flows. In: *AIAA 2005-0085*, Reno, pp 1–11
- [8] Eldredge JD, Wang C (2010) High-fidelity simulations and low-order modeling of a rapidly pitching plate. In: *AIAA 2010-4281*, Chicago, pp 1–19
- [9] Godoy-Diana R, Aider J-L, Wesfreid JE (2008) Transitions in the wake of a flapping foil. *Phys Rev E* 77:016308
- [10] Kanso E (2009) Swimming due to transverse shape deformations. *J Fluid Mech* 631:127–148
- [11] Kanso E, Marsden JE, Rowley CW, Melli-Huber JB (2005) Locomotion of articulated bodies in a perfect fluid. *J Nonlinear Sci* 15:255–289
- [12] Kern S, Koumoutsakos P (2006) Simulations of optimized anguilliform swimming. *J Exp Biol* 209:4841–4857
- [13] Krasny R (1989) Desingularization of periodic vortex sheet roll-up. *J Comput Phys* 65:292–313
- [14] Kolomenskiy D, Schneider K (2009) A Fourier spectral method for the Navier–Stokes equations with volume penalization for moving solid obstacles. *J Comp Phys* 228:5687–5709
- [15] Jones MA (2003) The separated flow of an inviscid fluid around a moving flat plate. *J Fluid Mech* 496:405–441
- [16] Jones MA, Shelley MJ (2005) Falling cards. *J Fluid Mech* 540:393–425
- [17] Michelin S, Llewellyn Smith SG (2009) An unsteady point vortex method for coupled fluid-solid problems. *Theor Comput Fluid Dyn* 23:127–153
- [18] Nitsche M, Krasny R (1994) A numerical study of vortex ring formation at the edge of a circular tube. *J Fluid Mech* 276:139–161
- [19] Pullin DI, Wang ZJ (2004) Unsteady forces on an accelerating plate and applications to hovering insect flight. *J Fluid Mech* 509:1–21

- [20] Rohr JJ, Fish FE (2004) Strouhal numbers and optimization of swimming by odontocete cetaceans. *J Exp Biol* 206:1633–1642
- [21] Schneider K (2005) Numerical simulation of the transient flow behaviour in chemical reactors using a penalization method. *Comput Fluid* 34:1223–1238
- [22] Schnipper T, Andersen A, Bohr T (2009) Vortex wakes of a flapping foil. *J Fluid Mech* 633:411–423
- [23] Shelley M, Alben S (2008) Flapping states of a flag in an inviscid fluid: bistability and the transition to chaos. *Phys Rev Lett* 100:074301
- [24] Shukla RK, Eldredge JD (2007) An inviscid model for vortex shedding from a deforming body. *Theor Comput Fluid Dyn* 21:343–368
- [25] Triantafyllou MS, Triantafyllou GS, Gophalkrishnan R (1991) Wake mechanics for thrust generation in oscillation foils. *Phys Fluid A* 3(12):2835–2837
- [26] Triantafyllou MS, Triantafyllou GS, Yue DKP (2000) Hydrodynamics of fishlike swimming. *Annu Rev Fluid Mech* 32:33–53
- [27] Wang ZJ (2000) Vortex shedding and frequency selection in flapping flight. *J Fluid Mech* 410:323–341
- [28] Ysasi A, Kanso E, Newton PK (2011) Wake structure of a deformable Joukowski airfoil. *Physica D* 240(20):1574–1582